Title
Disordered Structural Ensembles of Vasopressin and Oxytocin and Their Mutants

Journal
The Journal of Physical Chemistry B, 119(3)

ISSN
1520-6106

Authors
Yedvabny, Eugene
Nerenberg, Paul S
So, Clare
et al.

Publication Date
2015-01-22

DOI
10.1021/jp505902m

Peer reviewed

The Disordered Structural Ensembles of Vasopressin and Oxytocin and Their Mutants

Eugene Yedvabny[1], Paul S. Nerenberg[4], Clare So[2] and Teresa Head-Gordon[1,2,3*]

[1]Department of Chemistry, [2]Department of Bioengineering, [3]Department of Chemical and Biomolecular Engineering, University of California, Berkeley, CA 94720-3220 USA

[4]Division of Geological and Planetary Sciences, California Institute of Technology, Pasadena, CA 91125

***Corresponding author**

thg@berkeley.edu

ABSTRACT

Vasopressin and oxytocin are intrinsically disordered cyclic nonapeptides belonging to a family of neurohypophysial hormones. Although unique in their functions, these peptides differ only by two residues and both feature a tocin ring formed by the disulfide bridge between 1st and 6th cysteine residues. This sequence and structural similarity is experimentally linked to oxytocin agonism at vasopressin receptors and vasopressin antagonism at oxytocin receptors. Yet single-or double-residue mutations in both peptides have been shown to have drastic impacts on their activities at either receptor, and possibly the ability to bind to their neurophysin carrier protein. In this study we perform molecular dynamics simulations of the unbound native and mutant sequences of the oxytocin and vasopressin hormones in order to characterize their structural ensembles. We classify the sub-populations of these structural ensembles based on the distributions of radius of gyration and secondary structure and hydrogen-bonding features of the canonical tocin ring and disordered tail region. We then relate the structural changes observed in the unbound form of the different hormone sequences to experimental information about peptide receptor binding, and more indirectly, carrier protein binding affinity, receptor activity, and protease degradation. This study supports the hypothesis that the structural characteristics of the unbound form of an IDP can be used to predict structural or functional preferences of its functional bound form.

Keywords: Intrinsically disordered peptides, hormones, tocin ring, molecular simulation

INTRODUCTION

Intrinsically disordered peptides and proteins (IDPs) are biomolecules whose function is intimately related to their structural diversity. The characterization of IDP structural diversity is a challenge for traditional experimental methods, which have been finely honed on well-folded globular proteins. To address this problem, there has been recent progress in the reliable use of molecular dynamics (MD) to interpret the relevant sub-populations of IDPs once they are sufficiently validated against experimental data (primarily NMR). Previously we have applied MD to study the ensembles of amyloid-beta peptides in particular[1-5]. Here we extend these well-developed computational approaches to propose a structural interpretation of some puzzling functional behavior for two short IDP hormone peptides, oxytocin and vasopressin, and their mutants. Both are intrinsically disordered nonapeptide hormones that differ in sequence at two positions, CYIQNCPLG vs. CYFQNCPRG, respectively. Both hormones contain a disulfide bond between Cys^1 and Cys^6 that defines the so-called tocin ring, with an acyclic C-terminus tail that is amidated by post-translational modification as a means to control their bioactivity[6]. Crystal structures of the bound form of the native hormones to the neurophysin carrier proteins[7-8] shows that Tyr^2 of the native hormones is deeply buried in the neurophysin binding pocket, and thus it is likely that amino acid substitutions at this site would compromise the ability of the carrier protein to shepherd the peptides to their receptor targets.

Oxytocin is a potent hormone and neurotransmitter secreted within the pituitary gland, and is cleaved from a precursor along with its carrier protein neurophysin I. In addition to being used as an aid to induce labor, more recently oxytocin has been examined as a possible therapy for social anxiety disorders[9]. Because of its ability to unproductively interact with vasopressin receptors, considerable research has been directed toward synthetic peptide and non-peptide analogues with decreased turnover and increased receptor specificity. Previous studies identified a single-residue $Gln^4 \rightarrow Thr^4$ (Q4T) mutation in oxytocin that has twice as much binding and activity at the oxytocin receptor OXTR (also known as OTR) and only 10-25% as much activity at vasopressin receptors as the native peptide sequence.[10-12] When combined with a second mutation $Pro^7 \rightarrow Gly^7$ (P7G), however, the oxytocic activity is reduced to less than a third of the native peptide, while the vasopressin receptor activity becomes essentially immeasurable.[11-15]

The primary role of vasopressin is as an antidiuretic that regulates the concentration of water, glucose, and salts within blood. Vasopressin is secreted from the posterior pituitary and acts at a distance by binding to G protein-coupled AVPR2 (also known as V2R) receptors within the kidney that promote the insertion of aquaporin-2 channels into the membrane of epithelial cells within the kidney nephron collecting ducts[16]. While most forms of diabetes insipidus are caused by mutations in the neurophysin II carrier protein or in the vasopressin receptors located in the kidneys[17-21], more rare single mutation variants of vasopressin, $Tyr^2 \rightarrow His^2$ (Y2H) and $Pro^7 \rightarrow Leu^7$ (P7L), have been implicated in familial forms of diabetes insipidus[22-23]. Previous *in vitro* cell biology experiments carried out on the mutants of vasopressin, Y2H and P7L, by Christensen *et al.* suggested two independent pathogeneses of diabetes insipidus.[21] First that the Y2H mutation renders the hormone unable to be exported from the endoplasmic reticulum (likely due to its inability to bind correctly to its neurophysin II chaperone protein), greatly impairing its ability to leave the posterior pituitary and reach the receptors in the kidneys. In contrast, the P7L mutant is able to bind neurophysin and be successfully exported from the secretion granules in the posterior pituitary, likely due to the retention of Tyr^2. Instead, this experimental study hypothesized that the P7L mutation might result in conformational changes to the C-terminal region that could potentially hinder its ability to be processed from the pro-form by proteases.

Together, these biochemical data no doubt expose important determinants of receptor specificity, binding affinity to carrier proteins, bioactivity, and protease degradation, but on their own are not necessarily explicative. Several studies have previously characterized the structural motifs of native oxytocin and vasopressin using experimentally-restrained MD[24-27], which is different to our unrestrained MD approach and new emphasis on the structural properties of the aforementioned mutants. Although these intrinsically disordered peptides sample many different conformations, we hypothesize that specific structural properties of dominant sub-populations of the unbound peptides are essential contributors to the observed physiological behaviors. Our molecular dynamics simulations are shown to capture the variation in conformational ensembles due to mutations in these peptides, and by extension provide predictive evidence of which conformations may be important for binding and function. Here we explore the ability of MD simulations of the unbound peptides to explain the differences in receptor agonist activity of the parent vasopressin and oxytocin hormones, and to analyze the structural ensembles for possible mechanistic insight into the biological behavior of their mutants.

METHODS

The hormones were modeled using the AMBER ff99SB force field with improved ILDN side-chain torsions[28] and corrections for φ dihedral angles[29] and ω dihedral angles[30]. The peptides were solvated in explicit solvent represented by the TIP4P-Ew water model[31]. This combination of the adjusted ff99SB force field and TIP4P-Ew water model has been shown to better reproduce experimental NMR observables compared to other biomolecular simulation force fields[32-35].

The structural ensembles were produced from a Reservoir Replica Exchange (RREMD)[36] simulation performed with the AMBER 12 package[37]. All simulations used a 2 fs time step with SHAKE constraints on hydrogen vibrations, while a Langevin thermostat and a Berendsen barostat maintained the temperature and density respectively. Particle Mesh Ewald was used for calculating long-range electrostatic forces throughout the study, with a cutoff of 9.0 Å for the real space electrostatics and Lennard-Jones forces. We used the LEaP module to prepare the initial extended structures of the peptides and to solvate them with a 10 Å layer of water in a truncated-octahedron periodic box, with a total of 1500 water molecules. The charges on the peptides were neutralized with the addition of Cl^- counter ions. The systems were subsequently minimized and equilibrated to 298.15 K, first by heating from 0 K to the desired temperature under constant volume for 20 ps, followed by 300 ps of constant-pressure simulation at 1 bar to achieve the correct the density. The resulting equilibrated structures were then independently heated for 500 ps to 24 different temperatures, spanning from 298.15 K to 442.45 K, to generate the initial RREMD replicas.

In order to speed up convergence to the equilibrium distribution, we prepared a reservoir of 19500 representative structures for each peptide from last 195 ns of a 200-ns NVT simulation at 450 K using AMBER’s GPU-accelerated PMEMD.cuda module. Under the RREMD protocol, a random structure from the reservoir acts as a 25th replica during every other exchange attempt, seeding the simulation with pre-equilibrated proposals and thus reducing the convergence time. The production run consisted of 50 ns of NVT RREMD using the Sander module, with an exchange attempt every 0.5 ps, yielding a Boltzmann-weighted ensemble of 45000 structures evenly sampled from the last 45 ns of the simulation.

We used the cpptraj module of AMBER 14[38] to calculate the structural properties of the 298.15 K ensemble for all studied hormones. We imposed a 135° angle cutoff and a 3.5 Å distance cutoff between heavy atoms for identifying hydrogen bonds. The reported secondary structures were determined using the DSSP metric, which assigns structure types based off backbone amide and carbonyl positions.[39] The backbone chemical shifts for native oxytocin and vasopressin were determined using SHIFTX2[40] and reported as averages across the entire ensemble. The scalar couplings between the H_N and H_α atoms were calculated for all residues using the Karplus equation[41] from the φ dihedral angles, with a parameter set from Vuister and Bax[42], and likewise averaged across the ensemble. The uncertainties of SHIFTX2 and of the Karplus parameters are the dominant contributors to the uncertainties of the reported calculated observables.

RESULTS

Comparison of simulation to experiment. In order to validate our *de novo* structural ensembles, we compared the computed and experimental backbone chemical shifts and $^3J_{H\alpha HN}$ scalar couplings for native vasopressin and oxytocin. Experimental values were taken from a study by Sikorska *et al.*[24] for vasopressin, and from the comprehensive NMR analysis of Ohno *et al.*[43] for oxytocin. We have presented the chemical shift data in the form of a chemical shift index[44], in which residue-specific random coil chemical shifts[45] were subtracted from both the simulated and experimental data. As is evident from Figures 1, there is an overall good agreement between the majority of C_α, C_β, H_α and H_N chemical shifts. The three residues comprising the C-terminal tail of both peptides have experimental chemicals shifts very close to the random coil values, consistent with its much greater flexibility compared to the tocin ring[24, 43]. As shown in Tables 1 and 2, this trend is manifested in the structural ensembles, in which these residues show very low frequencies of persistent hydrogen bonds or secondary structure.

The tocin ring structure imposed by the Cys^1-Cys^6 cysteine disulfide bond, on the other hand, results in larger differences from random coil for the first six residues, which may be a signature of persistent structure. Our computed shifts reasonably reproduce these experimental differences for the most part, although the H_N and C_α chemical shifts at the 1, 4, and 6 residue positions show the largest deviation between the experimental and computed values for both peptides. The shift differences for both Cys^1 and Cys^6 are very likely due to deficiencies of the underlying parameters of the chemical shift calculators, which are trained on reduced cysteine rather than the oxidized form[40]. The fact that there is the same disagreement in chemical shift predictions for the same residues in both hormones may indicate systematic errors in the way chemical shift calculators handle short cyclic peptides, the unusual chemical environment of the tocin ring, and the greater amount of solvent exposure[46] of IDPs, although errors in the generated computational ensembles can not be ruled out either.

In addition to the chemical shifts, we compare the experimental scalar couplings to our simulated native oxytocin and vasopressin ensembles (Figure 2). As was the case with chemical shifts, we see a good match for the C-terminal tail, and qualitative agreement in the tocin ring, except for a flip in φ dihedral trends for Ile^3 to Gln^4 in oxytocin and Phe^3 to Gln^4 in vasopressin when compared to experiment. Overall, the underlying structural ensembles show reasonable agreement with experiment, although the NMR-based validation suite is not definitive. We have previously found that chemical shifts and J-coupling constants are not particularly useful for distinguishing between different IDP ensembles of amyloid-β peptides due to the conformational averaging that washes out distinctions between sub-populations[3]. Since there are presently no additional reported experimental studies (such as spin relaxation, residual dipolar couplings, SAXS etc) on these hormones to provide further points of comparison, we proceed with a more detailed analysis of the differences in the structural ensembles of vasopressin and oxytocin and their mutants as prediction to be tested by future refined experiments.

Classification of structural sub-populations. Figures 3 and 4 show the normalized radius of gyration (R_g) distributions for the native and mutant forms of oxytocin and vasopressin. When contrasting the native oxytocin and vasopressin peptides, the R_g distributions in both feature distinct sub-populations (or clusters) at 4.0-4.4 Å and 5.0-5.6Å, but exhibit differences in their secondary structure preferences and hydrogen-bond patterns within these sub-populations. Tables 1 and 2 report the secondary structure and dominant hydrogen bonds that are observed in the simulations for each nonapeptide, including the mutants, for the compact sub-population with R_g < 5.0 Å, and the extended sub-population with R_g > 5.0 Å.

Native Oxytocin vs. Vasopressin. From the simulated data, several generic features can be identified that explain the trends in receptor binding affinity of the two native peptides to their hormone receptors. The first is that oxytocin has a far greater percentage of extended structures relative to compact structures when compared to vasopressin. For both peptides, both the compact (Figure 5a) and extended (Figure 5b) sub-populations exhibit a ‘canonical’ tocin ring arrangement– a β–turn and α–turn stabilized by the Tyr^2-O to Asn^5-H and Tyr^2-O to Cys^6-H backbone hydrogen bonds. This bonding network is consistent with the ROESY-derived analysis by Sikorska *et al*[24], which found β–turn across residues 3-4 and 4-5 in native arginine vasopressin and mesotocin (an oxytocin analogue with Ile^8 replacing Leu^8). The compact sub-population is distinguished from the extended form by the presence of either a Cys^6-O to Gly^9-H or Pro^7-O Gly^9-H hydrogen bond. An NMR-constrained MD simulation by Sikorska *et al*[24] only saw the Cys^6-Gly^9 βIII turn in mesotocin, leading to a larger average R_g for vasopressin than mesotocin. Our ensembles, in contrast, feature the turn in the compact sub-population of both peptides, indicating even higher degree of homology across the peptides than previously reported. The strong similarities we observe for the ring motif and C-terminus structures of both hormones likely contributes to the cross-agonism between oxytocin and vasopressin and their receptors[10].

Nonetheless there are structural differences in the tocin ring when vasopressin is compared to oxytocin, in which vasopressin is structurally more diverse. In particular it adopts a higher percentage of a 3_{10} helix (actually a type III β–turn involving residues 2-5), a higher percentage of the 2-5 β–turn, a lower percentage of the 2-6 α–turn, and there is an appearance of a new hydrogen bond Phe^3-O to Cys^6-H in the extended population. Slusarz *et al.* have suggested that vasopressin binds to AVPR2 receptor through parallel aromatic sidechains of Tyr^2 and Phe^3, stabilized by Tyr^2-Asn^5, and hence the structural differences we observe in the tocin region for vasopressin relative to oxytocin may be important for AVPR2 receptor binding specificity[47-48].

Oxytocin and Mutants. The conformational ensemble of the Q4T oxytocin mutant is virtually identical to that of native oxytocin, in which the extended population is dominant for both, and is comprised of similar hydrogen bonds and secondary structure propensities in the extended form. The primary difference we observe between the native and Q4T mutant is a higher percentage of the compact structures, which is attributable to higher populations of the Cys^6-O to Gly^9-H and or Pro^7-O Gly^9-H hydrogen bonds. Furthermore, the mutant's compact sub-population exhibits a marked increase in the frequency of the canonical 2-5 β–turn and 2-6

α–turn, which may be consistent with the greater affinity of the Q4T peptide to OXTR compared to the native peptide, and this greater specificity for OXTR should at the same time reduce the affinity for the vasopressin receptor.

The Q4T/P7G double mutant shows a significant reduction in the extended cluster population, although this sub-population retains the tocin ring backbone hydrogen bond frequencies of the canonical 2-5 β–turn and 2-6 α–turn observed for native oxytocin. The retention of the canonical ring structure is consistent with experimental findings that Q4T/P7G maintains the specificity for the OXTR receptor. Instead the Q4T/P7G double mutant loses most of the specific structural features of the compact native ensemble, and instead exhibits a diversity of hydrogen-bond stabilized turns for both the tocin ring and C-terminus tail for this sub-population. The steep reduction to 11% for the 6-9 β–turn in the C-terminus of this compact cluster, in contrast to 50% and 71% of the compact ensembles of the native and single-mutant oxytocin, respectively, means that the tail can adopt new interactions with the tocin ring. These new interactions include a 3-7 α–turn and 4-7 β–turn, which may explain the reduced oxytocic activity as well as reduced vasopressin receptor activity[11-15].

Vasopressin and Mutants. Figure 4 compares the R_g distributions for native vasopressin and its mutants. For the Y2H mutant, the tyrosine of the tocin ring is replaced by a histidine residue, which has a side chain pKa of 6.04; this means that both protonated (Y2H+) and deprotonated (Y2H) forms of the side chain will be present *in vivo*, so we conducted simulations of both forms.

The R_g distribution for the Y2H mutant is not substantially different from the parent vasopressin hormone, although there is a greater percentage of extended structures, making it more similar to oxytocin. Overall the canonical 2-5 β–turn and 2-6 α–turn ring structure and C-terminal hydrogen bond populations do not differ dramatically from native vasopressin. However, the primary difference is that the histidine side chain forms a hydrogen bond with the tocin backbone nearly 82% of the time (Figure 6), meaning that it is unlikely to be found in an exposed conformation. In comparison, the tyrosine side chain of native vasopressin or oxytocin never forms a hydrogen bond with the backbone and thus is always exposed and available for carrier binding. Thus the histidine side chain of the Y2H mutant may be unable to fulfill the binding contact, and thus the carrier protein would be unable to shepherd this mutant form of the vasopressin peptide.

The R_g distribution for the Y2H+ mutant is seen to sample a very different conformational ensemble compared to native and the deprotonated mutant form, and is dominated by extended structures. There is a dramatic reduction in the frequencies of hydrogen bonds that define the canonical 2-5 β–turn and 2-6 α–turn tocin ring structure and compact C-terminal tail. For this mutant, the His^2 side chain also forms a hydrogen bond with the tocin backbone 28% of the time, reducing its likelihood of being found in an exposed conformation available for carrier binding. The population loss and restructuring of the entire conformational ensemble in solution would suggest that all binding and activity of the Y2H+ mutant would be compromised relative to native.

The P7L vasopressin mutant displays an R_g distribution unlike either form of the Y2H mutants or the native vasopressin and oxytocin peptides. There are no distinct compact and extended sub-populations, with most structures distributed fairly evenly across an R_g range of 4.6-6.2 Å. There is a catastrophic loss of the hydrogen bonds that define the canonical tocin ring of the native ensemble that would certainly lower the P7L mutant's binding affinity for the AVPR2 vasopressin receptor at the kidneys. Furthermore we see new tocin ring interaction with the tail, including the 3-7 α–turn and 4-7 β–turn observed for the oxytocin double mutant, which may also explain the reduced vasopressin receptor binding and activity.

Christensen et al have suggested that the P7L mutation might result in conformational changes to the C-terminal region that could potentially hinder proteases from excising the hormone from the pro-form[21]. We note that across all analyzed hormones, P7L had one the highest population of conformers within 2 Å RMSD to a trypsin-inhibiting structure of vasopressin (Table 3 and Figure 7), and thus might be capable of inhibiting the proteases responsible for cleaving the pro-form.

Role of Cis Isomer. The Pro^7 residue of both native oxytocin and vasopressin is unique amongst amino acids in its isoenergeticism between the *cis* and the *trans* conformations across the peptide bond. This allows a non-trivial population of the cis isomer under physiological conditions and the associated potential for interconversion. Based on 2D COSY NMR experiments, Larive *et al*[49] have demonstrated that the cis isomer comprises 10% of the *in vitro* populations of the two hormones at pH 3, although the NMR data from Sikorska et al[24] [43] (used for experimental comparison with the computed data) suggest that the cis isomer comprises only 5% for vasopressin. Furthermore, Wittelsberger *et al.*[50] have found that fixing the oxytocin Cys^6-Pro^7 peptide bond to the cis configuration resulted in 10-fold reduction in receptor agonism compared to the native hormone but no noticeable antagonism. The high activation barrier of the cis ↔ trans interconversion renders a dynamical simulation of the process computationally infeasible, however we considered an RREMD simulation comprising a 100% population of the cis conformation to understand what structural differences arise. Even at this high concentration of cis conformations, both the cis and trans ensembles yield virtually indistinguishable simulated chemical shift averages, prohibiting a conclusive determination of their relative populations (Figure 8).

The comparison of the Cys^6-Pro^7 trans and cis R_g distributions for the native oxytocin is presented in Figure 9. There is a marked shift in structural properties, with the cis distribution having a much higher percentage of compact conformations but also featuring an additional extended population not observed in the trans distribution. Although the Tyr^2-Asn^5 and Tyr^2-Cys^6 tocin backbone is still present in the majority of structures, the cis arrangement of the Cys^6-Pro^7 peptide bond positions the C-terminal tail closer to the tocin ring. The tail Gly^9 now forms a hydrogen bond with the ring Gln^4 in over 20% of the ensemble, resulting in a reduction in the canonical tocin ring structure but a growth in β–turn across residues 6-8. These deformations of the ring and the tail are similar to the ones observed for the oxytocin double-mutant, furthering the hypothesis that the canonical ring structure is key to oxytocin receptor specificity and activity.

Variation in Protein Force Fields. The development of modern fixed-charge force fields has reached a point where *de novo* biophysical simulations of proteins are able to consistently reproduce and characterize experimental observables with a remarkable level of accuracy. Nonetheless, the classical assumptions underlying these force fields are constantly improved through reparameterization, which is especially important for small disordered peptides that are more solvent exposed and have fewer stabilizing protein-protein interactions compared to their folded counterparts.

Figure 10 depicts the R_g distribution of native oxytocin modeled with the unmodified AMBER ff99SB force field[51] and with the ff99SB+ILDN+φ+ω used in this study. The ff99SB ensemble features an extended sub-population, centered around 6.5 Å, that is entirely absent from the distribution derived from the newest AMBER parameter set that is currently considered to be one of the best protein force fields available. This new sub-population is lacking the canonical Tyr^2-Asn^5 and Tyr^2-Cys^6 ring backbone hydrogen bonds, which are key factors to oxytocin receptor binding. The only dominant secondary structure is a β–turn configuration across Tyr^2-Ile^3, in only 30% of the structures in the sub-population, formed by backbone hydrogen bonds between Cys^1 or Tyr^2 and Gln^4. Conversely, the structural properties of the 4.3 Å and 5.4 Å sub-populations remain largely conserved across the two force fields, both prominently featuring the Tyr^2-Asn^5 and Tyr^2-Cys^6 hydrogen bonds and the α–turn across Ile^3-Asn^5.

Though the disappearance of the most extended conformation in native oxytocin is the most drastic impact of a force field change observed in the course of this study, all seven hormones exhibited some smaller degree of variation across the force fields. These variations underlie the importance of constant improvement to the force-field parameters, and the progress gained in the six years between the release of ff99SB and of the modified ILDN, φ, and ω parameters. Based off a better agreement between the experimental NMR observables calculated for the f99SB+ILDN+φ+ω ensemble, as well as the numerous validations of the corrections in other simulations, we believe the findings reported in this study using the newer force field represent the more accurate structural ensembles for vasopressin, oxytocin, and their mutants.

DISCUSSION AND CONCLUSION

Computational studies by Slusarz *et al* on docking of the hormones to their receptors[47-48] have suggested that the selectivity of oxytocin to OXTR is largely dependent on receptor interactions with Tyr^2, Ile^3, and Leu^8, while vasopressin binds to the AVPR2 receptor through parallel aromatic sidechains of Tyr^2 and Phe^3. We find that there are subtle structural differences between oxytocin and vasopressin in the types and frequencies of turns that are adopted across residues that define the tocin ring and C-terminus, and that these changes may be tied to this selectivity. This observation stems directly from the use of unrestrained MD, which allows for characterization of energetically-allowed conformations that do not necessarily conform to the *averaging* nature of such restraints. Furthermore our data support a structural hypothesis that the Q4T oxytocin mutant increases both the binding specificity and the activity at the G protein-coupled OXTR receptor due to ‘rigidification’ of the tocin ring backbone, evident in the greater population of the canonical 2-5 β–turn and 2-6 α–turn compared to native, and reduces the structural features of the tocin ring needed to recognize the vasopressin receptors.

Conversely, the addition of the second mutation, $Pro^7 \rightarrow Gly^7$ (Q4T/P7G), retains the high frequency of Tyr^2-Asn^5 and Tyr^2-Cys^6 bonds and the canonical tocin turn propensities that makes it a competent binder to the receptor, but the loss of canonical structure in the C-terminus is the most obvious factor that would reduce its bioactivity relative to the native peptide. Instead a new α−turn and β−turn couple the tocin ring to the C-terminus which may explain the observed reduction in both the oxytocin and vasopressin receptor activity[11-15]. While our simulations cannot elaborate on the hypothesis that the *cis-trans* isomerization about the Cys^6-Pro^7 peptide bond is essential to the activation of OXTR receptor[50], it is likely that orientation of the C-terminus tail is a determining factor in the hormone’s ability to activate the receptor post-binding, and thus this mutant may not be competent for this role.

Whereas the native vasopressin features an exposed Tyr^2 phenol side-chain without being encumbered by other intramolecular interactions, His^2 of the Y2H and Y2H+ ensembles is most often found bonded to Gln^4 or Asn^5 and thus unable to act as a binding site for neurophysin II.

While we find that the protonated form Y2H+ would also be compromised for leaving the pituitary, we would also predict that it would be an incompetent binder at the receptor due to loss of the canonical structure in the tocin ring. The P7L mutant, on the other hand, is readily exported from the ER due to retention of Tyr^2, which suggests that it has a similar ability to bind neurophysin II as native vasopressin. Therefore P7L's lack of antidiuretic function is likely due either to an inability for proteases to cleave it in its prohormone state or a reduced binding affinity/activation ability at the AVPR2 receptor. Our simulation results aligned with both of the hypothesized disease mechanisms for this mutant.

The field of intrinsically disordered peptides and proteins revolves around the extent to which structural motifs in the disordered conformational ensemble are important for function and disease. Our *de novo* MD simulations show that even small nonapeptide hormones, such as oxytocin and vasopressin, exhibit well-defined hydrogen bonding patterns and secondary structure motifs in the majority of observed structures that deviate from the random-coil behavior often attributed to IDPs[1-3]. While the focus of this study is mainly on oxytocin and vasopressin and their mutants, we note that our underlying hypothesis is that the structural determinants of the *unbound* hormonal peptides that are disordered will have sub-populations of structure that overlaps with the bound form of the ordered peptide. Thus the relevance of this work also touches on how to interpret the functional significance of the disordered structural ensemble, which remains an open question. We note that a recent combined NMR-MD study found that certain conformational sub-populations in the free-state ensemble of the IDP Gab2 was predictive for the binding motif exhibited by bound receptor complex Grb[52]. However, another study found that residual structure in the isolated form of the intrinsically disordered PUMA protein was unimportant for its binding the folded protein MCL-1[53].

We conclude that the effects of the shifts in structural patterns we observe across the unbound native and mutant oxytocin and vasopressin hormones correlate well with observed changes in receptor activity and physiological function, including possible receptor binding motifs. As such, this computational study supports the hypothesis that the structural characteristics of the unbound form of an IDP can be used to predict structural or functional preferences of its functional bound form.

ACKNOWLEDGEMENTS

The work reported here is supported by resources of UC Berkeley CITRIS and the National Energy Research Scientific Computing Center, which is supported by the Office of Science of the U.S. Department of Energy under Contract No. DE-AC02-05CH11231. THG thanks the NSF for support under grant CHE-1265731. THG also acknowledges computational resources obtained under NSF grant CHE-1048789. THG would like to thank Bill for his many insightful scientific accomplishments that have proved foundational to the field of molecular simulation. The authors declare no conflict of interest.

SUPPORTING INFORMATION AVAILABLE: Details on the structural ensembles by residue and simulation convergence profile. This material is available free of charge via the Internet at http://pubs.acs.org.

REFERENCES

1. Ball, K. A.; Phillips, A. H.; Nerenberg, P. S.; Fawzi, N. L.; Wemmer, D. E.; Head-Gordon, T., Homogeneous and heterogeneous tertiary structure ensembles of amyloid-beta peptides. *Biochemistry* **2011**, *50*, 7612-28.

2. Ball, K. A.; Phillips, A. H.; Wemmer, D. E.; Head-Gordon, T., Differences in β-strand populations of monomeric amyloid-β 40 and amyloid-β 42. *Biophys. J.* **2013**, *104*, 2714-2724.

3. Ball, K. A.; Wemmer, D. E.; Head-Gordon, T., Comparison of Structure Determination Methods for Intrinsically Disordered Amyloid-β Peptides. *J. Phys. Chem. B* **2014**, *118*, 6405–6416.

4. Fawzi, N. L.; Yap, E. H.; Okabe, Y.; Kohlstedt, K. L.; Brown, S. P.; Head-Gordon, T., Contrasting disease and nondisease protein aggregation by molecular simulation. *Acc Chem Res* **2008**, *41*, 1037-47.

5. Fawzi, N. L.; Phillips, A. H.; Ruscio, J. Z.; Doucleff, M.; Wemmer, D. E.; Head-Gordon, T., Structure and dynamics of the Abeta(21-30) peptide from the interplay of NMR experiments and molecular simulations. *J Am Chem Soc* **2008**, *130*, 6145-58.

6. Du Vigneaud, V.; Ressler, C.; Trippett, S., The sequence of amino acids in oxytocin, with a proposal for the structure of oxytocin. *J Biol Chem* **1953**, *205*, 949-57.

7. Rose, J. P.; Wu, C.-K.; Hsiao, C.-D.; Breslow, E.; Wang, B.-C., Crystal structure of the neurophysin—oxytocin complex. *Nature Structural Biology* **1996**, *3*, 163-169.

8. Wu, C. K.; Hu, B.; Rose, J. P.; Liu, Z. J.; Nguyen, T. L.; Zheng, C.; Breslow, E.; Wang, B. C., Structures of an unliganded neurophysin and its vasopressin complex: implications for binding and allosteric mechanisms. *Protein Sci* **2001**, *10*, 1869-80.

9. Theodoridou, A.; Penton-Voak, I. S.; Rowe, A. C., A direct examination of the effect of intranasal administration of oxytocin on approach-avoidance motor responses to emotional stimuli. *PloS one* **2013**, *8*, e58113.

10. Manning, M.; Stoev, S.; Chini, B.; Durroux, T.; Mouillac, B.; Guillon, G., Peptide and non-peptide agonists and antagonists for the vasopressin and oxytocin V1a, V1b, V2 and OT receptors: research tools and potential therapeutic agents. *Progress in Brain Research* **2008**, *170*, 473-512.

11. Lowbridge, J.; Manning, M.; Haldar, J.; Sawyer, W. H., Synthesis and some pharmacological properties of [4-threonine, 7-glycine] oxytocin,[1-(L-2-hydroxy-3-mercaptopropanoic acid), 4-threonine, 7-glycine] oxytocin (hydroxy [Thr4, Gly7] oxytocin), and [7-Glycine] oxytocin, peptides with high oxytocic-antidiuretic selectivity. *Journal of medicinal chemistry* **1977**, *20*, 120-123.

12. Barberis, C.; Morin, D.; Durroux, T.; Mouillac, B.; Guillon, G.; Seyer, R.; Hibert, M.; Tribollet, E.; Manning, M., Molecular pharmacology of AVP and OT receptors and therapeutic potential. *Drug News Perspect* **1999**, *12*, 279-292.

13. Bespalova, Z. D.; Martynov, V.; Titov, M., New oxytocin analoguess7-Glycine-oxytocin and 7-D-leucine-oxytocin. *Zh. Obs. Khim* **1968**, *38*, 1684-1687.

14. Bodansky, M.; Bath, R. J., Hindered amines in peptide synthesis. Synthesis of 7-glycine-oxytocin. *Chemical Communications (London)* **1968**, 766-767.

15. Walter, R.; Yamanaka, T.; Sakakibara, S., A neurohypophyseal hormone analog with selective oxytocin-like activities and resistance to enzymatic inactivation: an approach to the design of peptide drugs. *Proceedings of the National Academy of Sciences* **1974**, *71*, 1901-1905.

16. Nielsen, S.; Chou, C. L.; Marples, D.; Christensen, E. I.; Kishore, B. K.; Knepper, M. a., Vasopressin increases water permeability of kidney collecting duct by inducing translocation of aquaporin-CD water channels to plasma membrane. *Proceedings of the National Academy of Sciences of the United States of America* **1995**, *92*, 1013-7.

17. Elias, P. C.; Elias, L. L.; Torres, N.; Moreira, A. C.; Antunes-Rodrigues, J.; Castro, M., Progressive decline of vasopressin secretion in familial autosomal dominant neurohypophyseal diabetes insipidus presenting a novel mutation in the vasopressin-neurophysin II gene. *Clinical endocrinology* **2003**, *59*, 511-518.

18. Bergeron, C.; Kovacs, K.; Ezrin, C.; Mizzen, C., Hereditary diabetes insipidus: an immunohistochemical study of the hypothalamus and pituitary gland. *Acta neuropathologica* **1991**, *81*, 345-348.

19. Wolf, M.; Dötsch, J.; Metzler, M.; Holder, M.; Repp, R.; Rascher, W., A new missense mutation of the vasopressin-neurophysin II gene in a family with neurohypophyseal diabetes insipidus. *Hormone Research in Paediatrics* **2003**, *60*, 143-147.

20. Christensen, J. H.; Siggaard, C.; Corydon, T. J.; Kovacs, L.; Robertson, G. L.; Gregersen, N.; Rittig, S., Six novel mutations in the arginine vasopressin gene in 15 kindreds with autosomal dominant familial neurohypophyseal diabetes insipidus give further insight into the pathogenesis. *European journal of human genetics* **2004**, *12*, 44-51.

21. Christensen, J. H.; Siggaard, C.; Corydon, T. J.; Robertson, G. L.; Gregersen, N.; Bolund, L.; Rittig, S., Differential cellular handling of defective arginine vasopressin (AVP) prohormones in cells expressing mutations of the AVP gene associated with autosomal dominant and recessive familial neurohypophyseal diabetes insipidus. *The Journal of clinical endocrinology and metabolism* **2004**, *89*, 4521-31.

22. Willcutts, M. D.; Felner, E.; White, P. C., Autosomal recessive familial neurohypophyseal diabetes insipidus with continued secretion of mutant weakly active vasopressin. *Human molecular genetics* **1999**, *8*, 1303-1307.

23. Rittig, S.; Siggaard, C.; Ozata, M.; Yetkin, I.; Gregersen, N.; Pedersen, E. B.; Robertson, G. L., Autosomal dominant neurohypophyseal diabetes insipidus due to substitution of histidine for tyrosine2 in the vasopressin moiety of the hormone precursor. *Journal of Clinical Endocrinology & Metabolism* **2002**, *87*, 3351-3355.

24. Sikorska, E.; Rodziewicz-Motowidło, S., Conformational studies of vasopressin and mesotocin using NMR spectroscopy and molecular modelling methods. Part I: Studies in water. *Journal of peptide science : an official publication of the European Peptide Society* **2008**, *14*, 76-84.

25. Liwo, A.; Tempczyk, A.; Oldziej, S.; Shenderovich, M. D.; Hruby, V. J.; Talluri, S.; Ciarkowski, J.; Kasprzykowski, F.; Lankiewicz, L.; Grzonka, Z., Exploration of the conformational space of oxytocin and arginine-vasopressin using the electrostatically driven Monte Carlo and molecular dynamics methods. *Biopolymers* **1996**, *38*, 157-75.

26. Hagler, A. T.; Osguthorpe, D. J.; Dauber-Osguthorpe, P.; Hempel, J. C., Dynamics and conformational energetics of a peptide hormone: vasopressin. *Science* **1985**, *227*, 1309-15.

27. Ward, D. J.; Chen, Y.; Platt, E.; Robson, B., Development and testing of protocols for computer-aided design of peptide drugs, using oxytocin. *J Theor Biol* **1991**, *148*, 193-227.

28. Lindorff-Larsen, K.; Piana, S.; Palmo, K.; Maragakis, P.; Klepeis, J. L.; Dror, R. O.; Shaw, D. E., Improved side-chain torsion potentials for the Amber ff99SB protein force field. *Proteins* **2010**, *78*, 1950-8.

29. Nerenberg, P. S.; Head-Gordon, T., Optimizing Protein−Solvent Force Fields to Reproduce Intrinsic Conformational Preferences of Model Peptides. *Journal of Chemical Theory and Computation* **2011**, *7*, 1220-1230.

30. Doshi, U.; Hamelberg, D., Reoptimization of the AMBER force field parameters for peptide bond (Omega) torsions using accelerated molecular dynamics. *The journal of physical chemistry. B* **2009**, *113*, 16590-5.

31. Horn, H. W.; Swope, W. C.; Pitera, J. W.; Madura, J. D.; Dick, T. J.; Hura, G. L.; Head-Gordon, T., Development of an improved four-site water model for biomolecular simulations: TIP4P-Ew. *The Journal of chemical physics* **2004**, *120*, 9665-78.

32. Beauchamp, K. a.; Lin, Y.-S.; Das, R.; Pande, V. S., Are Protein Force Fields Getting Better? A Systematic Benchmark on 524 Diverse NMR Measurements. *Journal of chemical theory and computation* **2012**, *8*, 1409-1414.

33. Best, R. B.; Buchete, N.-V.; Hummer, G., Are Current Molecular Dynamics Force Fields too Helical? *Biophysical Journal* **2008**, *95*, L07-L09.

34. Best, R. B.; Hummer, G., Optimized Molecular Dynamics Force Fields Applied to the Helix−Coil Transition of Polypeptides. *The Journal of Physical Chemistry B* **2009**, *113*, 9004-9015.

35. Wickstrom, L.; Okur, A.; Simmerling, C., Evaluating the Performance of the ff99SB Force Field Based on NMR Scalar Coupling Data. *Biophysical Journal* **2009**, *97*, 853-856.

36. Okur, A.; Roe, D. R.; Cui, G.; Hornak, V.; Simmerling, C., Improving Convergence of Replica-Exchange Simulations through Coupling to a High-Temperature Structure Reservoir. *Journal of Chemical Theory and Computation* **2007**, *3*, 557-568.

37. D.A. Case, T. A. D., T.E. Cheatham, III, C.L. Simmerling, J. Wang, R.E. Duke, R.; Luo, R. C. W., W. Zhang, K.M. Merz, B. Roberts, S. Hayik, A. Roitberg, G. Seabra,; J. Swails, A. W. G., I. Kolossváry, K.F. Wong, F. Paesani, J. Vanicek, R.M. Wolf, J. Liu,; X. Wu, S. R. B., T. Steinbrecher, H. Gohlke, Q. Cai, X. Ye, J. Wang, M.-J. Hsieh, G.; Cui, D. R. R., D.H. Mathews, M.G. Seetin, R. Salomon-Ferrer, C. Sagui, V. Babin, T.; Luchko, S. G., A. Kovalenko, P.A. Kollman *AMBER 12*, University of California, San Francisco, 2012.

38. D.A. Case, V. B., J.T. Berryman, R.M. Betz, Q. Cai, D.S. Cerutti, T.E. Cheatham, III, T.A. Darden, R.E. Duke, H. Gohlke, A.W. Goetz, S. Gusarov, N. Homeyer, P. Janowski, J. Kaus, I. Kolossváry, A. Kovalenko, T.S. Lee, S. LeGrand, T. Luchko, R. Luo, B. Madej, K.M. Merz, F. Paesani, D.R. Roe, A. Roitberg, C. Sagui, R. Salomon-Ferrer, G. Seabra, C.L. Simmerling, W. Smith, J. Swails, R.C. Walker, J. Wang, R.M. Wolf, X. Wu and P.A. Kollman *AMBER 14*, University of California, San Francisco, 2014.

39. Kabsch, W.; Sander, C., Dictionary of protein secondary structure: pattern recognition of hydrogen-bonded and geometrical features. *Biopolymers* **1983**, *22*, 2577-637.

40. Han, B.; Liu, Y.; Ginzinger, S. W.; Wishart, D. S., SHIFTX2: significantly improved protein chemical shift prediction. *Journal of biomolecular NMR* **2011**, *50*, 43-57.

41. Karplus, M., Contact Electron-Spin Coupling of Nuclear Magnetic Moments. *The Journal of Chemical Physics* **1959**, *30*, 11.

42. Vuister, G. W.; Bax, A., Quantitative J correlation: a new approach for measuring homonuclear three-bond J(HNH.alpha.) coupling constants in 15N-enriched proteins. *Journal of the American Chemical Society* **1993**, *115*, 7772-7777.

43. Ohno, A.; Kawasaki, N.; Fukuhara, K.; Okuda, H.; Yamaguchi, T., Complete NMR analysis of oxytocin in phosphate buffer. *Magnetic Resonance in Chemistry* **2010**, *48*, 168-72.

44. Wishart, D. S.; Sykes, B. D., The 13C Chemical-Shift Index: A simple method for the identification of protein secondary structure using 13C chemical-shift data. *Journal of Biomolecular NMR* **1994**, *4*, 171-180.

45. Schwarzinger, S.; Kroon, G. J.; Foss, T. R.; Wright, P. E.; Dyson, H. J., Random coil chemical shifts in acidic 8 M urea: implementation of random coil shift data in NMRView. *Journal of biomolecular NMR* **2000**, *18*, 43-8.

46. Xu, X. P.; Case, D. A., Automated prediction of (15)N, (13)C(alpha), (13)C(beta) and (13)C ' chemical shifts in proteins using a density functional database. *Journal of Biomolecular Nmr* **2001**, *21*, 321-333.

47. Slusarz, M. J.; Giełdoń, A.; Slusarz, R.; Ciarkowski, J., Analysis of interactions responsible for vasopressin binding to human neurohypophyseal hormone receptors-molecular dynamics study of the activated receptor-vasopressin-G(alpha) systems. *Journal of Peptide Science* **2006**, *12*, 180-189.

48. Slusarz, M. J.; Slusarz, R.; Ciarkowski, J., Molecular dynamics simulation of human neurohypophyseal hormone receptors complexed with oxytocin-modeling of an activated state. *Journal of Peptide Science* **2006**, *12*, 171-179.

49. Larive, C. K.; Guerra, L.; Rabenstein, D. L., Cis/trans conformational equilibrium across the cysteine6-proline peptide bond of oxytocin, arginine vasopressin, and lysine vasopressin. *Journal of the American Chemical Society* **1992**, *114*, 7331-7337.

50. Wittelsberger, A.; Patiny, L.; Slaninova, J.; Barberis, C.; Mutter, M., Introduction of a cis-prolyl mimic in position 7 of the peptide hormone oxytocin does not result in antagonistic activity. *Journal of medicinal chemistry* **2005**, *48*, 6553-62.

51. Hornak, V.; Abel, R.; Okur, A.; Strockbine, B.; Roitberg, A.; Simmerling, C., Comparison of multiple Amber force fields and development of improved protein backbone parameters. *Proteins* **2006**, *65*, 712-25.

52. Krieger, J. M.; Fusco, G.; Lewitzky, M.; Simister, P. C.; Marchant, J.; Camilloni, C.; Feller, S. M.; De Simone, A., Conformational recognition of an intrinsically disordered protein. *Biophys. J.* **2014**, *106*, 1771-1779.

53. Rogers, J. M.; Wong, C. T.; Clarke, J., Coupled folding and binding of the disordered protein PUMA does not require particular residual structure. *J. Amer. Chem. Soc.* **2014**, *136*, 5197-5200.

54. Syed, I. B.; Pattabhi, V., Trypsin inhibition by a peptide hormone: crystal structure of trypsin-vasopressin complex. *Journal of Molecular Biology* **2005**, *348*, 1191-1198.

55. Pettersen, E. F.; Goddard, T. D.; Huang, C. C.; Couch, G. S.; Greenblatt, D. M.; Meng, E. C.; Ferrin, T. E., UCSF Chimera--a visualization system for exploratory research and analysis. *J Comput Chem* **2004**, *25*, 1605-12.

TABLES

Table 1. We report the percentage of structures within each sub-ensemble of the native and mutant hormones that exhibited a particular type a hydrogen bond. Statistics for compact conformation are taken from dominant sup-populations with $R_g < 5$ Å and those for extended are taken from sub-population with $R_g > 5$ Å.

Hormone/ Hydrogen-Bonds	*Oxy Native*	*Oxy Q4T*	*Oxy Q4T/P7G*	*Vaso Native*	*Vaso Y2H*	*Vaso Y2H+*	*Vaso P7L*
Tyr2(His)-O Cys6-H (compact)	68%	84%		60%	77%	16%	16%
Tyr2(His)-O Cys6-H (extended)	79%	84%	73%	41-63%	80%	19%	8%
Tyr2(His)-O Asn5-H (compact)	74%	86%		92%	87%	74%	32%
Tyr2(His)-O Asn5-H (extended)	82%	79%	88%	89-91%	81%	62%	41-44%
Ile3-O Gly7-H (extended)			12%				
Phe3-O Cys6-H (extended)				17%			19-22%
Cys6-O Gly9-H (compact)	50%	71%	11%	31%	31%	58%	
Pro7(Leu7)-O Cter- H (compact)	14%	29%		36%	33%		
Gln4-OE1 Gln4-H (compact)	15%						
His2-ND1 Gln4-H (all)					82%		
His2-HD1-Asn5-OD1 (all)						28%	

Table 2. We report the percentage of structures within each sub-ensemble of the native and mutant hormones that exhibited a particular type a DSSP[39] secondary structure. Statistics for compact conformation are taken from dominant sup-populations with R_g < 5 Å and those for extended are taken from sub-population with R_g > 5 Å.

Hormone/ 2º structure	*Oxy Native*	*Oxy Q4T*	*Oxy Q4T/P7G*	*Vaso Native*	*Vaso Y2H*	*Vaso Y2H+*	*Vaso P7L*
β-turn 2-5, α-turn 2-6 (compact)	84%	98%		87-91%	98%	55-97%	42-60%
β-turn 2-5, α-turn 2-6 (extended)	92%	95%	80%	72-92%	97%	58-91%	47-76%
β-turn 6-9 (compact)	67%	90%		63%	68%	77%	22%
3-10 helix 2-5 (compact)	2.5%	1.2%		8.7%	<1%	1.1%	4%
3-10 helix 2-5 (extended)	3.6%	1.6%	5%	8-23%	1.6%	3.0%	17%
α-helix 3-6 (all)			24%				5-20%
α-turn 3-7; β-turn 4-7 (compact)			14-18%		1.6%		34%
β-bridge (2 and 5) (all)						2.3%	8%
β-bridge (6 and 9) (all)						4.0%	1%
β-bridge (3 and 6) (all)						7.2%	2.0%

Table 3: Structural backbone RMSD to trypsin-inhibiting vasopressin (1YF4)[54]. Alignment was performed on backbone C, C_α, N and O atoms.

Hormone	*R_g bounds (Å)*	*Min RMSD (Å)*	*% ensemble within 2.5 Å*
Native oxytocin	4.0-4.62	1.50	0.9
	5.0-5.7	0.93	5.1
Q4T oxytocin	3.9-4.3	1.50	0.6
	5.0-5.6	0.97	2.8
Q4T,P7G oxytocin	5.13-5.5	1.05	2.7
Native vasopressin	4.1-4.43	2.12	0.4
	4.95-5.6	1.92	3.9
	5.7-6.0	2.16	2.3
Y2H vasopressin	4.0-4.48	1.79	0.6
	4.85-5.67	1.69	2.8
Y2H+ vasopressin	4.2-4.48	1.74	3.8
	5.45-6.25	1.25	40.2
P7L vasopressin	4.5-4.9	1.52	2.3
	5.0-5.5	1.64	11.0
	5.7-6.1	1.44	35.6

FIGURE CAPTIONS

Figure 1a. *Experimental and calculated native oxytocin proton and carbon chemical shift indices by residue.* Experimental values taken from Ohno *et al.*[43] Residue-specific random coil chemical shifts[45] are subtracted from both the calculated and experimental values.

Figure 1b. *Experimental and calculated native vasopressin proton and carbon chemical shift indices by residue.* Experimental values taken from Sikorska *et a*l.[24] Residue-specific random coil chemical shifts[45] are subtracted from both the calculated and experimental values.

Figure 2. *J-coupling constants for backbone amides of native oxytocin and vasopressin.* Red squares represent the experimental values taken from Ohno *et al.*[43] and Sikorska *et al.*[24] respectively. Black circles represent the calculated coupling constants from the simulated ensemble.

Figure 3. *Radius of gyration (R_g) distributions for native and mutant oxytocin forms*.

Figure 4. *Radius of gyration (R_g) distributions for native and mutant vasopressin forms*.

Figure 5. *Representative snapshot of the canonical tocin ring conformation for* (a) the compact structure stabilized by a β–turn in the C-terminus, and (b) the extended conformation that is disordered. Only the backbone is shown. The disulfide bridge is shown in yellow. Green dashes represent the dominant 2-5 and 2-6 hydrogen bonds and the stabilizing 6-9 bond. Figures generated with UCSF Chimera[55].

Figure 6. *Representative snapshot of the interactions of His[2] with Gln[4] for the Y2H mutants*. Only the backbone is shown with the exception of His[2]. The disulfide bridge is shown in yellow. Green dashes represent the dominant 2-5 and 2-6 hydrogen bonds and the sidechain-backbone bond. Figure generated with UCSF Chimera[55].

Figure 7. *A dominant conformation for P7L that closely resembles the hormone bound state with the trypsin protease inhibitor*. The averaged backbone structure of P7L is in red and the 1YF4 vasopressin backbone is in blue. Figure generated with UCSF Chimera[55].

Figure 8. *Calculated backbone carbon and proton chemical shift indices for Cys^{6}-Pro^{7} trans and cis isomers of native oxytocin.* Residue-specific random coil chemical shifts[45] are subtracted from both sets of data. The difference in C_β for Pro^{7} is due to different random coil carbon shifts for the two configurations of the sidechain.

Figure 9. *Radius of gyration (R_g) distributions for Cys^{6}-Pro^{7} trans and cis isomers of native oxytocin.*

Figure 10. *Radius of gyration (R_g) distributions for ensembles of native oxytocin simulated under two different force fields*: ff99SB+ILDN+φ+ω and ff99SB.

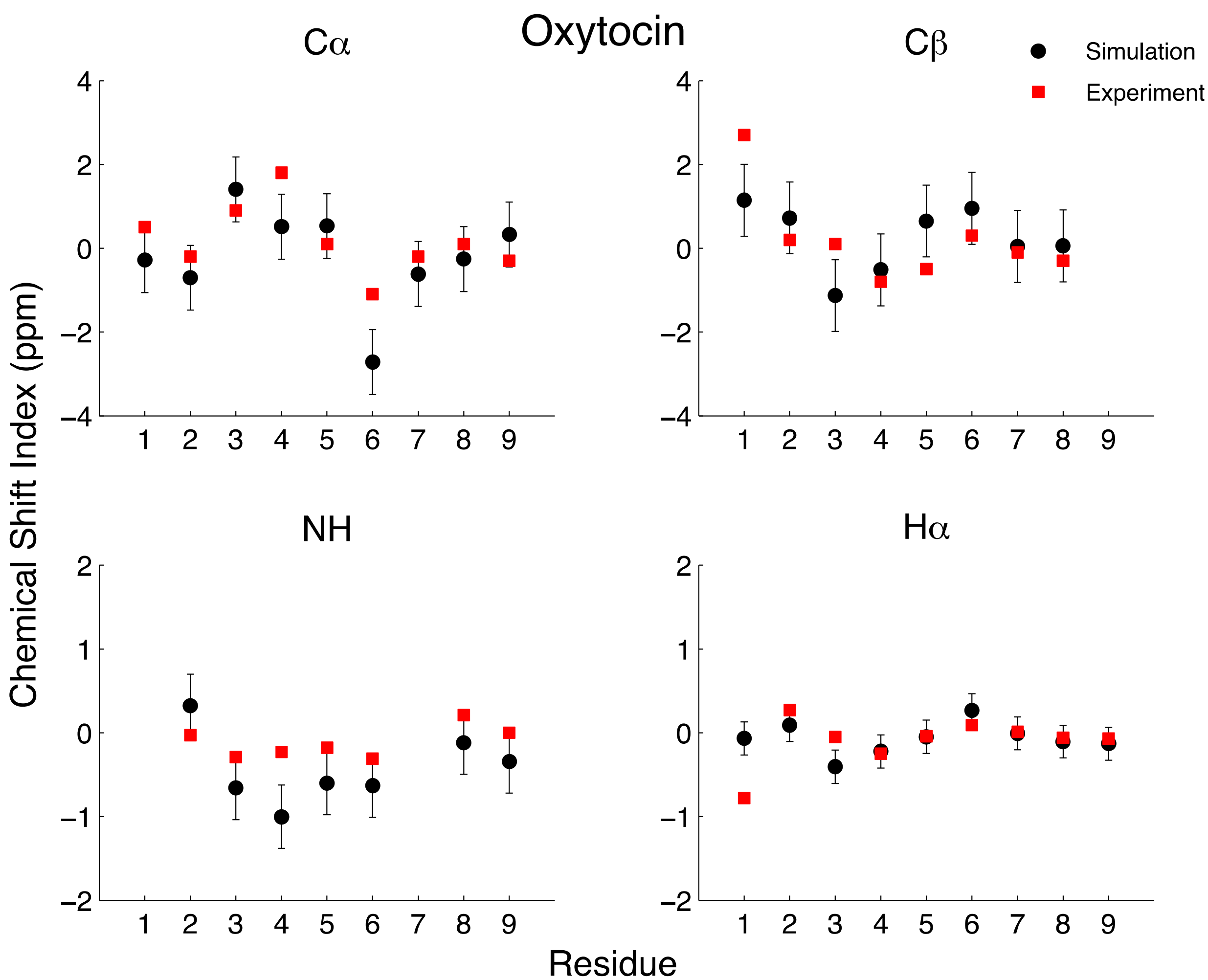

Figure 1a. Yedvabny and co-workers

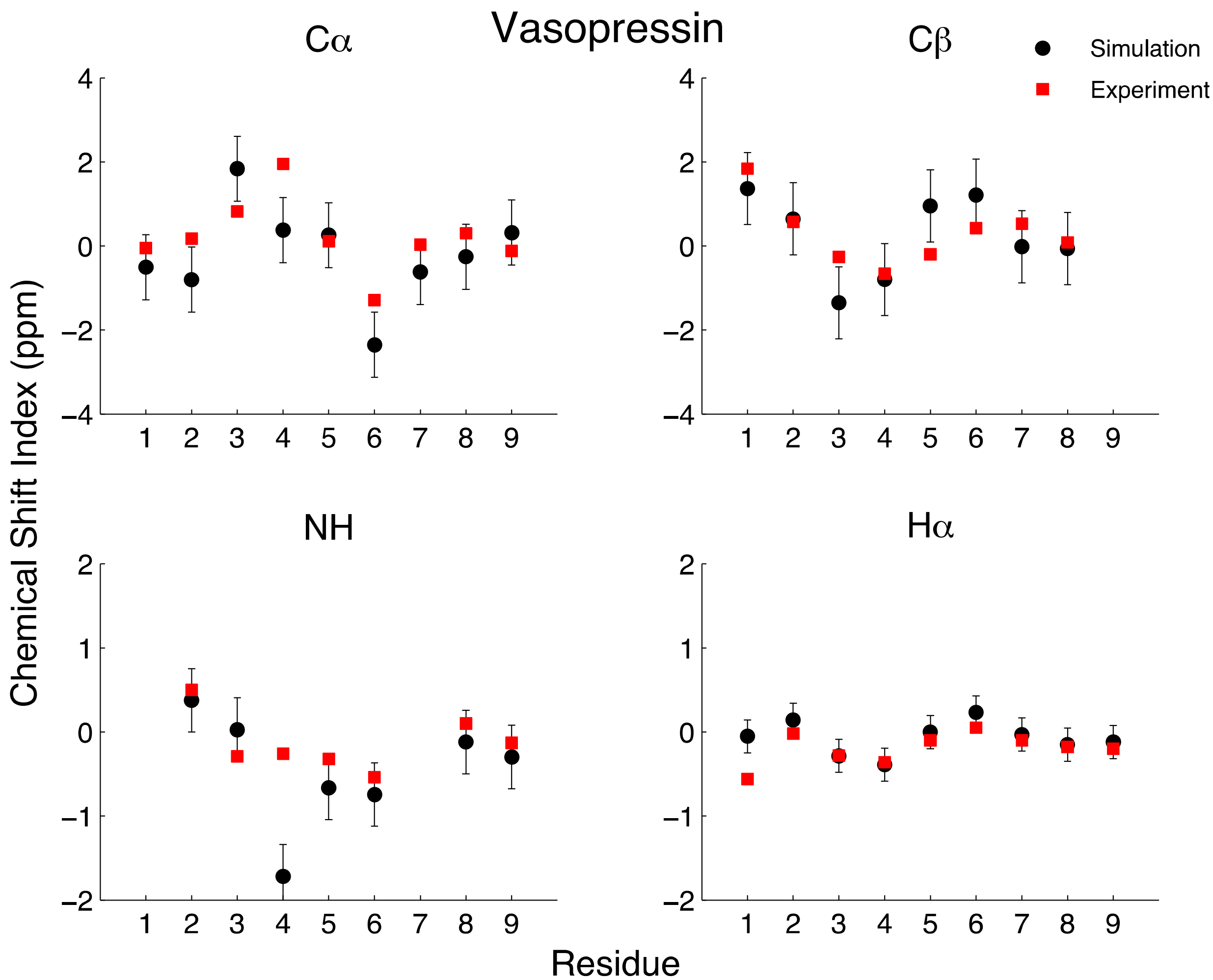

Figure 1b. Yedvabny and co-workers

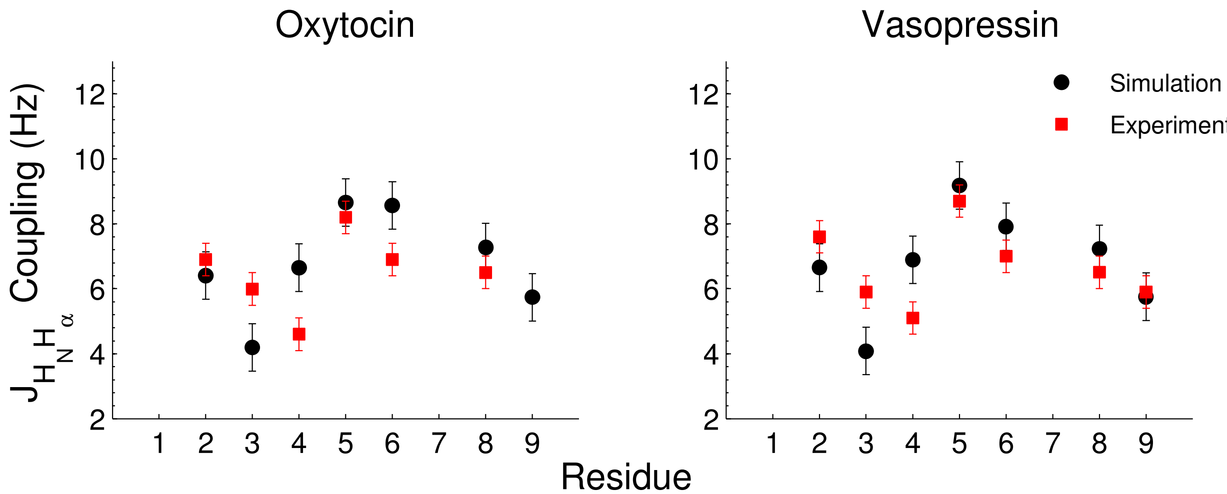

Figure 2. Yedvabny and co-workers

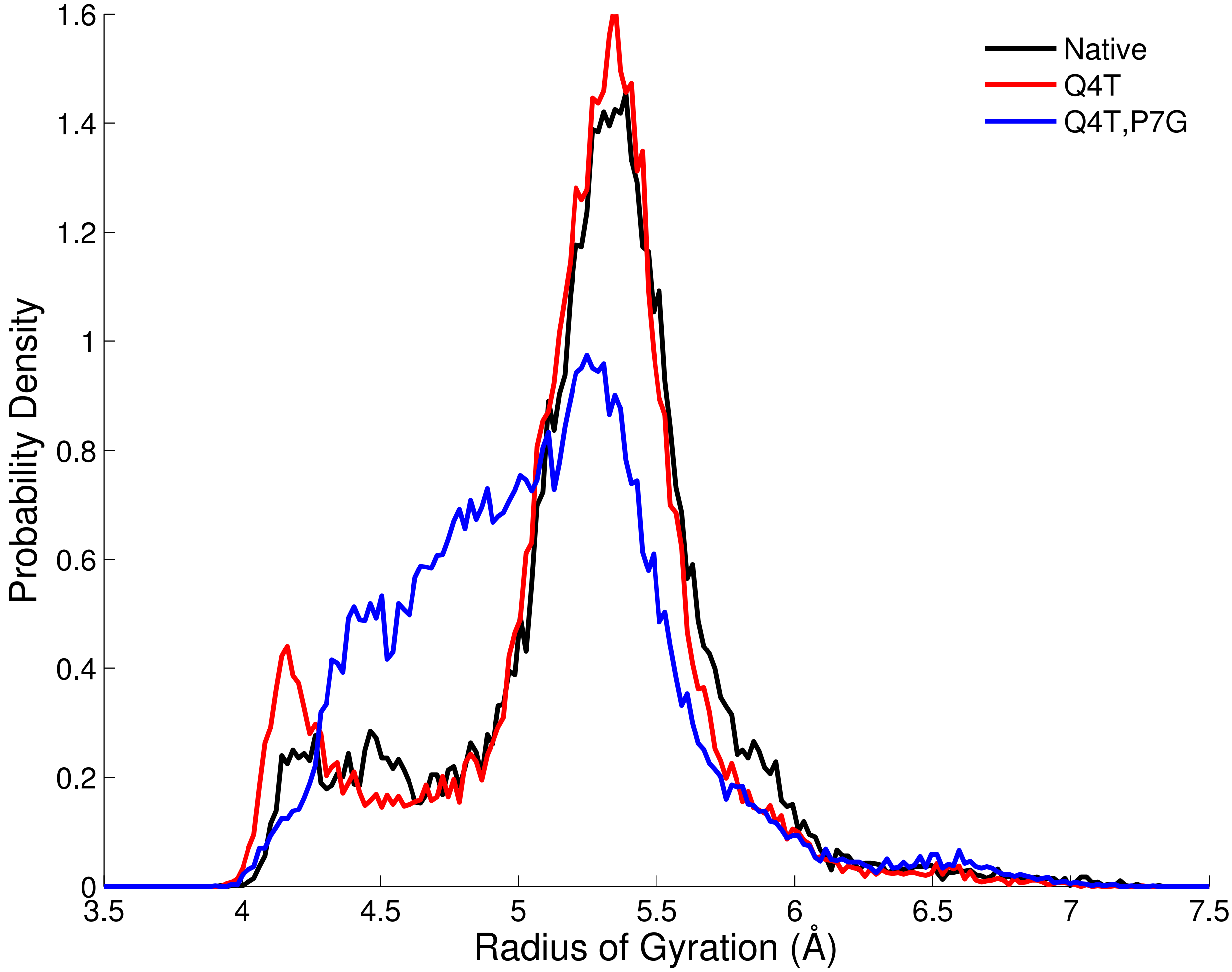

Figure 3. Yedvabny and co-workers

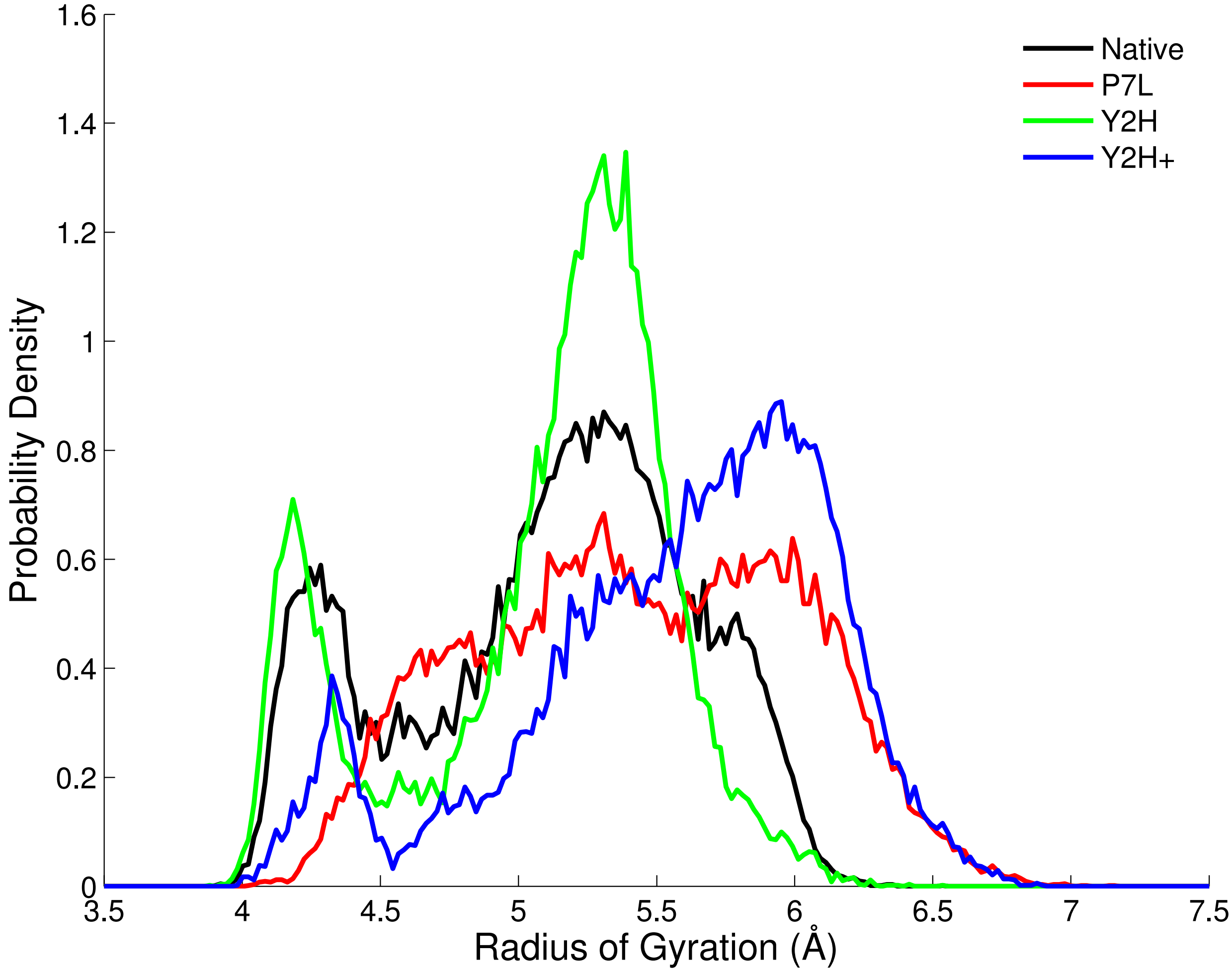

Figure 4. Yedvabny and co-workers

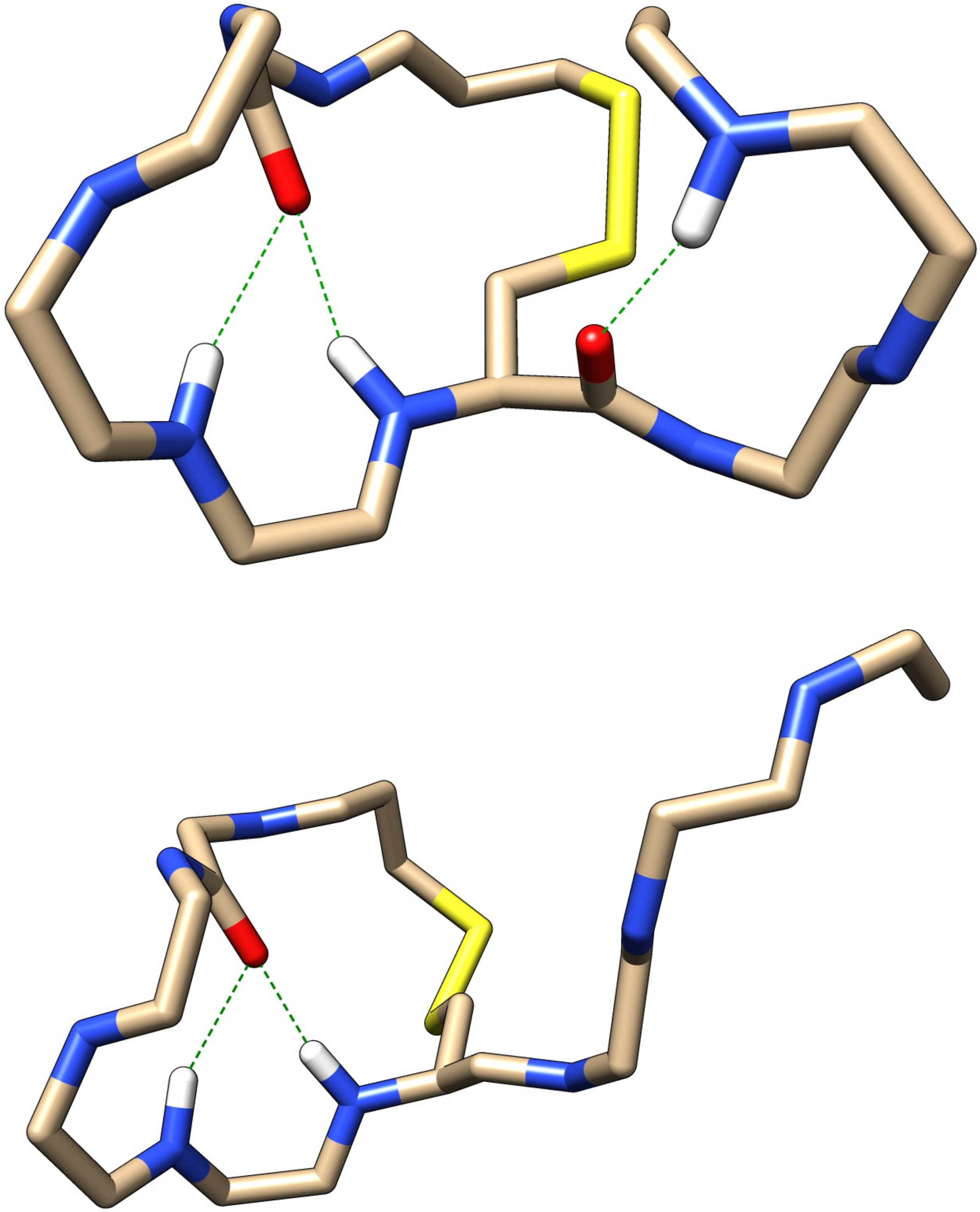

Figure 5. Yedvabny and co-workers

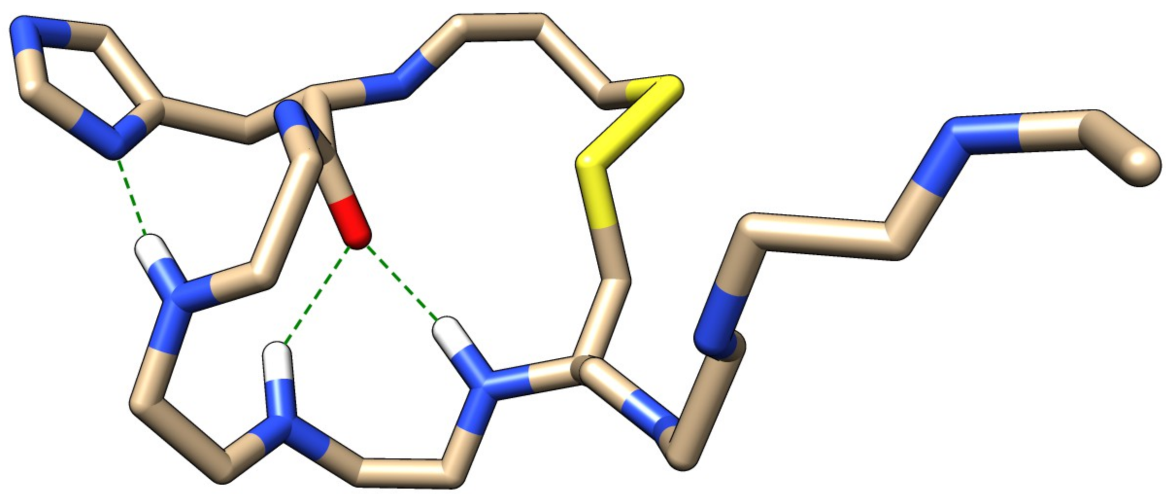

Figure 6. Yedvabny and co-workers

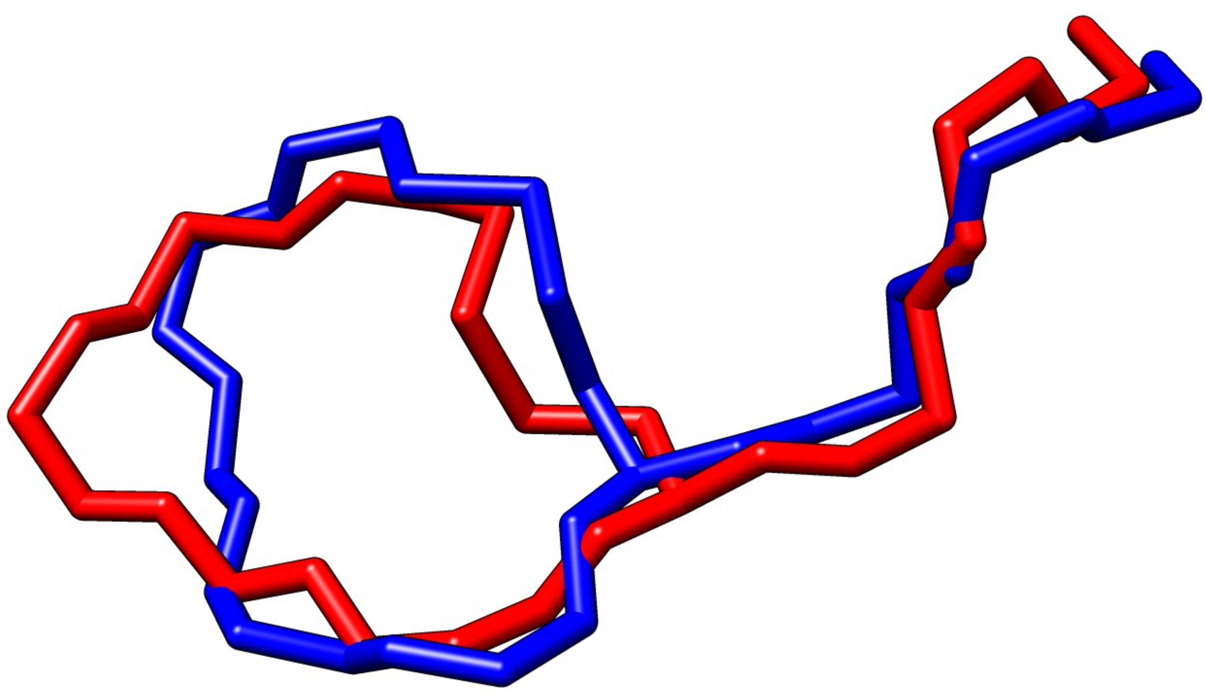

Figure 7. Yedvabny and co-workers

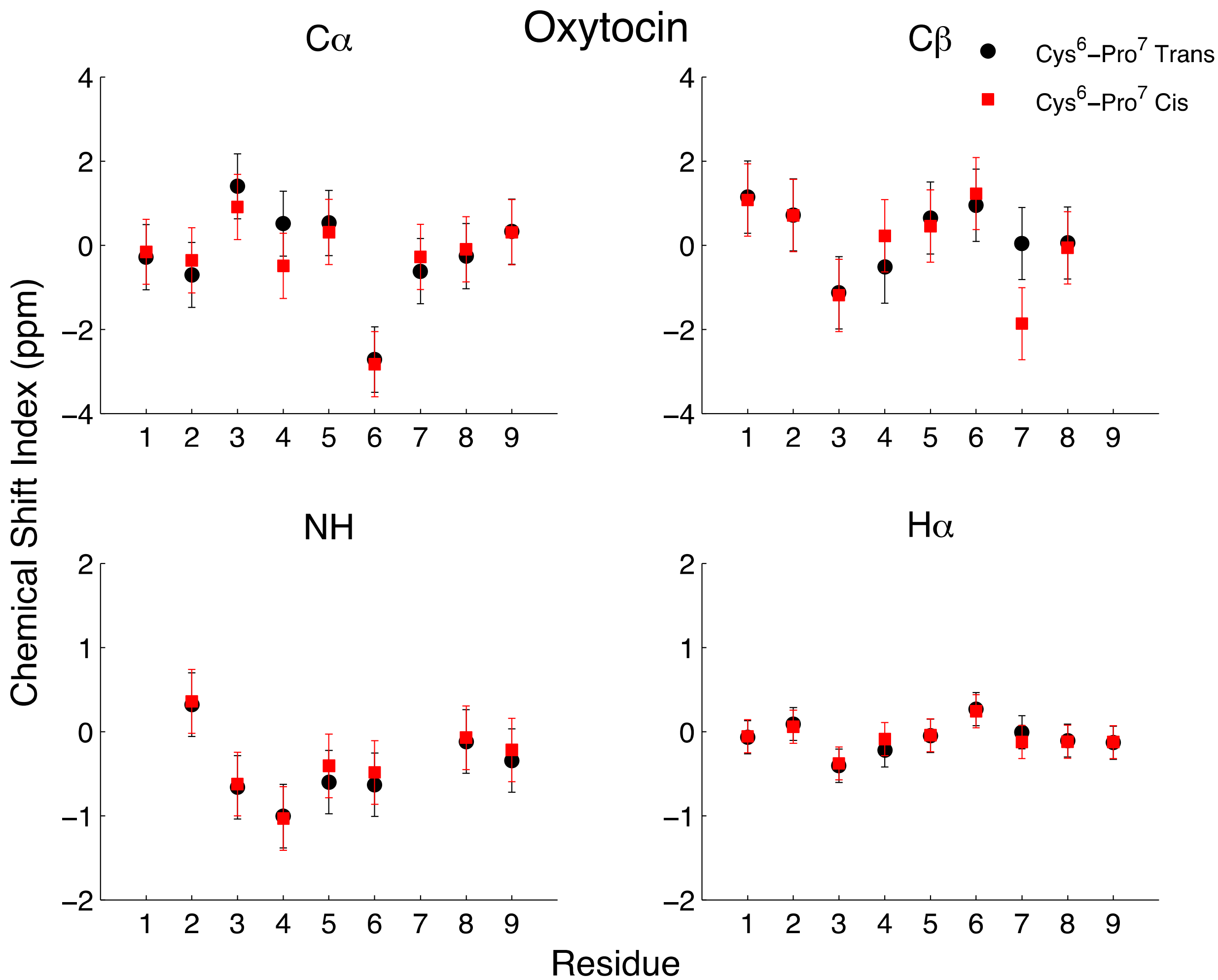

Figure 8. Yedvabny and co-workers

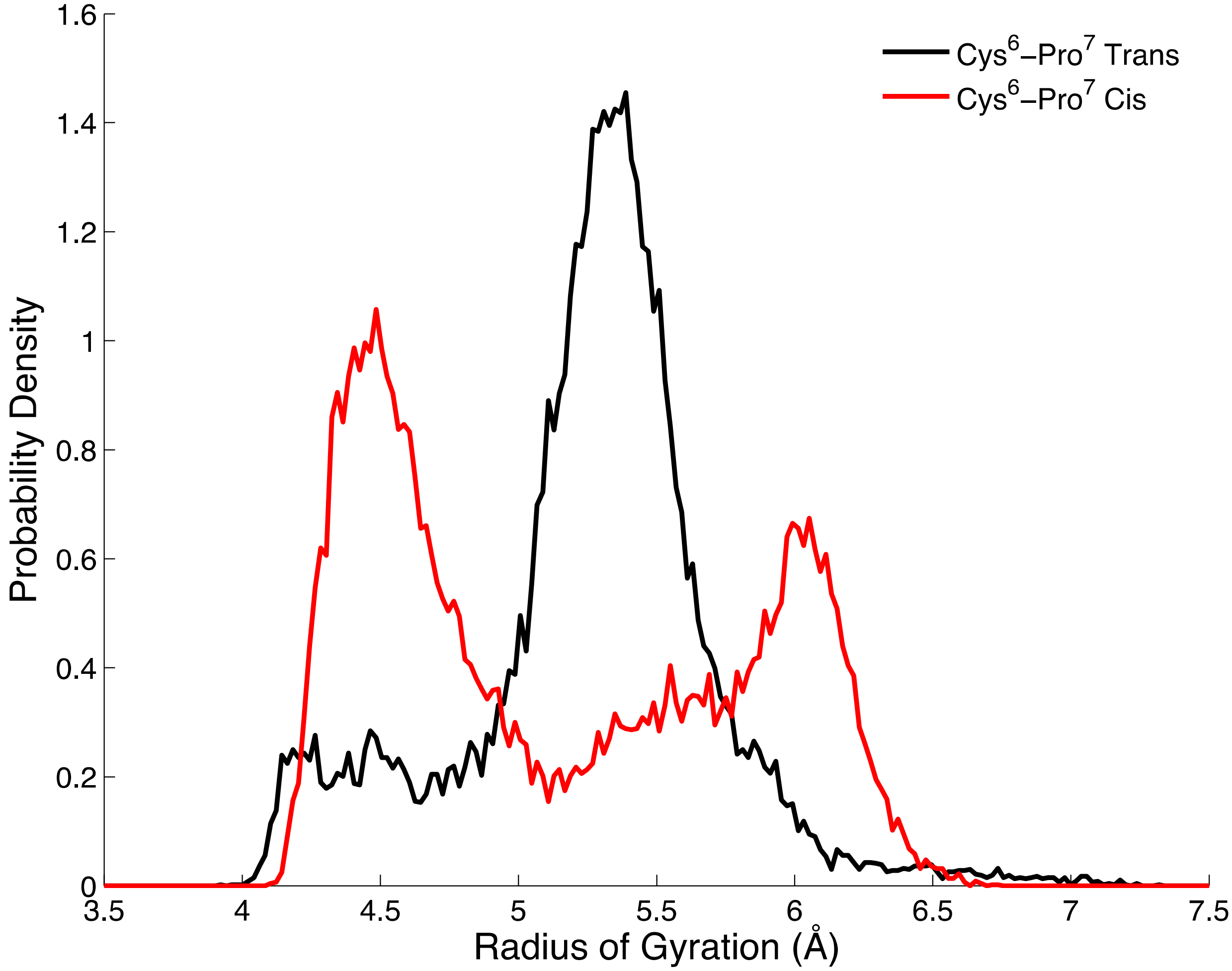

Figure 9. Yedvabny and co-workers

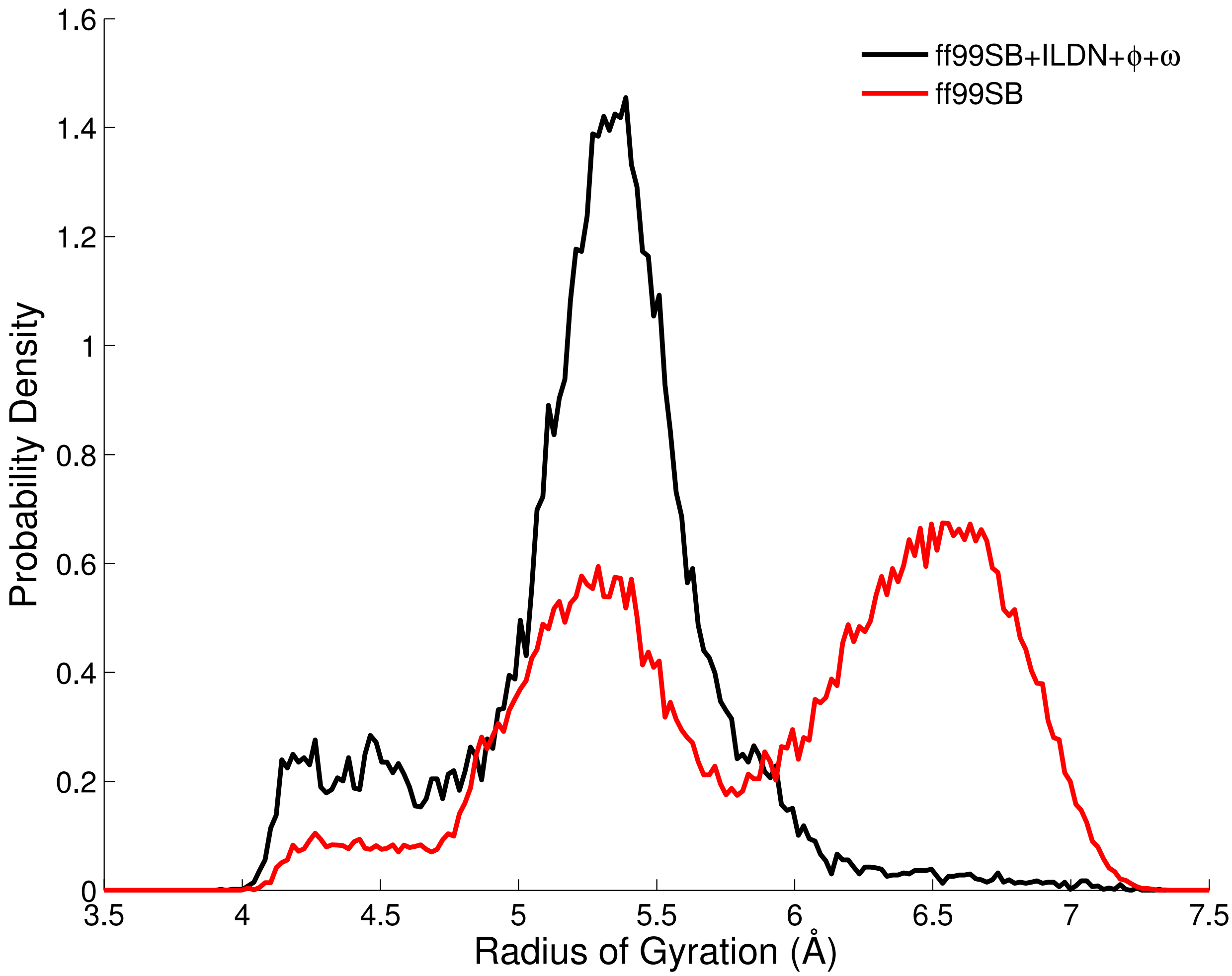

Figure 10. Yedvabny and co-workers

TOC FIGURE: